Energy 52 (2013) 201–209

Contents lists available at SciVerse ScienceDirect

Energy

journal homepage: www.elsevier.com/locate/energy

# A dynamic model for thermoelectric generator applied in waste heat recovery

Xiaolong Gou*, Suwen Yang, Heng Xiao, Qiang Ou

*School of Power Engineering, Chongqing University, Chongqing 400044, China*

ARTICLE INFO

*Article history:*
Received 15 July 2012
Received in revised form
22 December 2012
Accepted 18 January 2013
Available online 13 February 2013

*Keywords:*
Dynamic model
Thermoelectric generator
Waste heat recovery

ABSTRACT

Thermoelectric devices can provide clean energy conversion and are environmentally friendly. However, few studies have been conducted to understand the dynamic characteristics of (thermoelectric generators) TEGs. The stability of output performance plays a very important role in TEG. Based on the thermoelectric effect and heat transfer theory, a dynamic model for waste heat recovery in a general TEG was developed to asses the influence of heat reservoir and heat sink. The validity of the theoretical model was demonstrated by experiments and it was found that the model prediction agrees well with the experimental results. The dynamic response characteristics, such as hot and cold semiconductor surface temperatures, maximum output power and system efficiency, were studied using this dynamic model. The results showed that enhancing heat dissipation on cold side is the crucial to improve the output performance of TEG, and that the fluctuation of hot reservoir leads to rapid change of output power generated by TEG, which is dangerous to electric devices. The dynamic model proposed in the present study can be used in the design and operation analysis of TEGs.



## 1. Introduction

As energy shortage and environmental deterioration are growing, energy saving and emission reduction have become global obligation and responsibility. Besides being environmentally friendly, the thermoelectric technology has many other advantages such as being highly reliable, adapting to different kinds of heat reservoirs and having no moving parts. Therefore, the generation technology has received more and more attention in scientific community, especially in the aspect of waste heat recovery [1].

In order to improve the energy conversion efficiency of TEG, researchers have completed a number of experimental and modeling studies. Niu et al. [2] setup a low-cost, simple configuration TEG unit with commercially available $Bi_2Te_3$ based on the (thermoelectric module) TEM for an anticipated maximum power generation of about 150–200 W. Casano and Piva [3] analyzed TEG on the basis of the experimental data for 'open' and 'closed' circuit voltage, electric power output and conversion efficiency as a function of temperature.

In the case of simulated study, a numerical model with taking contact effects and actual structure into account was developed by Liang et al. [4]. It was found that the matched load of TEG was not equal to the internal resistance. Hsiao et al. [5] applied a mathematic model of thermoelectric module with applications on waste heat recovery from automobile engine to establish fundamental analyses of TEM. Zhou [6] presented a two-stage TEG, analyzed and optimized the performance in the objective function of efficiency and output power. And Chen et al. [7] analyzed the effects of design factors on the performance of the two-stage TEG, and they presented a novel configuration for a two-stage thermoelectric heat pump system driven by a two-stage TEG [8]. The effect of the heat transfer irreversibility on the performance of TEG was also researched [9,10]. In consideration of temperature dependence of thermoelectric properties and external heat transfer irreversibility, Chen et al. [11] established a new model of multi-element thermoelectric generator. The results show that the temperature dependence of thermoelectric properties has a significant effect on the power, efficiency and optimal variables of TEG. A linear phenomenological heat transfer model [12] and a radiative heat transfer model [13] were also presented by Chen et al. Hsu et al. [14] deliberated the issue how to transform the energy of waste heat into electricity for vehicles and motorcycles.

In addition, some authors not only have conducted experimental studies, but also developed simulating models. Crane and Jackson [15] focused on simultaneously optimizing both the heat exchanger geometry and the thermoelectric geometry for optimal net waste heat recovery performance. In our previous study, we have also conducted an optimization on low-temperature waste heat thermoelectric generator system by experiment and modeling [16].

Most of the researchers focused on the static properties of TEGs, and few studies on the dynamic characteristics have been carried

* Corresponding author. Tel.: +86 23 6510 3512; fax: +86 23 6510 2473.
*E-mail address:* simgxl@cqu.edu.cn (X. Gou).

0360-5442/$ – see front matter © 2013 Elsevier Ltd. All rights reserved.
http://dx.doi.org/10.1016/j.energy.2013.01.040

**Nomenclature**

| | |
|---|---|
| $A$ | area ($m^2$) |
| $c_p$ | specific heat capacity (J $kg^{-1}$ $K^{-1}$) |
| $E$ | electromotive force (V) |
| $h$ | convective heat transfer coefficient (W $m^{-2}$ $K^{-1}$) |
| $H$ | height (m) |
| $I$ | electric current (A) |
| $K$ | thermal conductance (W/K) |
| $l$ | length (m) |
| $n$ | number |
| $P$ | perimeter (m), power (W) |
| $q$ | heat flux ($W/m^2$) |
| $q_v$ | inner heat generation per unit volume ($W/m^3$) |
| $Q$ | heat transfer rate (W) |
| $Q_v$ | inner heat generation (W) |
| $r$ | electric resistance (Ω) |
| $R$ | thermal resistance (K/W) |
| $S$ | surface |
| $T$ | temperature (K) |
| $u$ | velocity (m/s) |
| $W$ | flow rate ($m^3/h$) |
| $y$ | coordinate |

*Greek letters*

| | |
|---|---|
| $\alpha$ | Seebeck coefficient (V/K) |
| $\delta$ | thickness (m) |
| $\eta$ | efficiency (%) |
| $\lambda$ | thermal conductivity (W $m^{-1}$ $K^{-1}$) |
| $\rho$ | density ($kg/m^3$) |
| $v$ | Kinematic viscosity coefficient ($m^2/s$) |
| $\tau$ | time (s) |
| $\Delta$ | difference |

*Subscripts*

| | |
|---|---|
| a | air |
| b | base |
| $a/b$ | material |
| c | cold, channel |
| ce | ceramic substrate |
| ch | characteristic length |
| con | contact |
| conv | convective heat transfer |
| cu | copper conducting strip |
| ef | effective |
| ex | heat exchanger |
| f | fin |
| fc | flow channel |
| h | hot |
| i | inner |
| L | load |
| m | matched |
| max | maximum |
| N | N-type semiconductor |
| P | P-type semiconductor |
| sc | semiconductor |
| sl | solder layer |
| ss | stainless steel |
| w | water |

*Abbreviation*

| | |
|---|---|
| *Nu* | Nusselt number |
| *Pr* | Prandtl number |
| *Re* | Reynolds number |
| th | hyperbolic tangent function |

out. Moreover, the TEG output performance is susceptible to heat reservoir. The running process is an extremely unstable process in practice, when taking waste heat as the hot reservoir of a TEG; meanwhile, the stability of output performance plays a very important role in TEG. Therefore, it is essential to study the TEG dynamic response characteristics along with changes of heat reservoirs.

In this study, a theoretical dynamic model of a thermoelectric generator for waste heat recovery has been built. At the same time, a corresponding thermoelectric device is constructed to validate the model. Based on the dynamic model, the TEG dynamic response characteristics have been modeled when temperatures and flow rates of heat reservoirs follow step changes.

## 2. System modeling

According to Seebeck effect, the TEG open-circuit voltage depends mainly on the temperature difference between the cold and hot sides of semiconductor. That is to say, changes of the temperature difference lead to changes of the open-circuit voltage, and the TEG output performance will change as well. Therefore, the unsteady-state heat transfer model is built to solve the TEG temperature distribution first. And the TEG dynamic model is setup after the corresponding performance calculation model is built.

### 2.1. Unsteady-state heat transfer model [17]

To build the unsteady-state heat transfer model, it is essential to conduct an unsteady-state the heat transfer analysis first. Similar with Ref. [17], the basic configuration for the TEG dynamic study follows the general design illustrated in Fig. 1. Thermoelectric modules are sandwiched between heat exchanger and flow channel with hot fluid that can be treated as a convective heat transfer system.

A TEM consists of two ceramic substrates, a certain number of semiconductors, corresponding solder layers, copper conducting strips and thermal insulation material, as illustrated in Fig. 2. The semiconductors are connected thermally in parallel, but electrically in series.

For a well-designed thermal insulation packing TEM, the heat leakage through the TEM surrounding could be neglected.

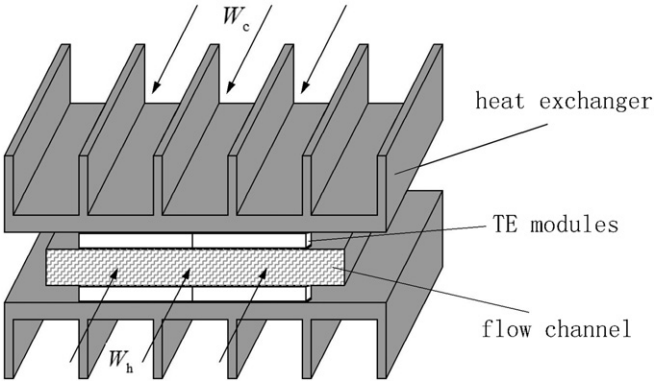


**Fig. 1.** The general design of thermoelectric system.

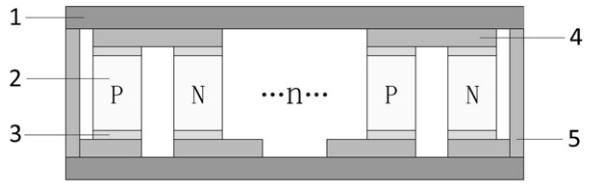


**Fig. 2.** A thermoelectric module.

Furthermore, both the specific heat capacity and the volume of air in TEM are so small that the heat leakage through the surrounding of TEM parts could also be neglected. In addition, the temperature differences between TEM parts are small because temperature of hot reservoir studied is not high. So the radiation heat transfer in TEM could be neglected. Therefore, the TEG model can be processed in a one-dimensional heat transfer way, as shown in Fig. 3.

According to heat conduction theory, the one-dimensional unsteady heat conduction equation on the hypothesis of physical parameter being constant can be shown as [18]:

$$\rho c_p \frac{\partial T}{\partial \tau} = \lambda \frac{\partial^2 T}{\partial y^2} + q_v \tag{1}$$

where $\rho$, $c_p$ and $\lambda$ are density, specific heat capacity and thermal conductivity respectively, $\tau$ and $y$ are time and axis coordinate respectively, and $q_v$ is inner heat generation per unit volume.

Unlike common power generation technology, the thermoelectric generator involves three basic effects, Seebeck effect, Peltier effect and Thomson effect. Besides, there are two accessorial effects, Joule effect and Fourier effect. Seebeck effect generates electromotive force. Peltier effect, Thomson effect and Joule effect lead to Peltier heat, Thomson heat and Joule heat, respectively. Therefore, the TEG inner heat generation includes Peltier heat, Thomson heat and Joule heat, which are conducted an analyzed in the following.

Firstly, Peltier heat generates on the two sides of semiconductor, so it can be disposed as the boundary heat flux. Secondly, Thomson heat is small enough to be neglected since it is a second-round effect. Finally, Joule heat can be regarded as flowing equally to the two sides of conductors [19], so it can also be disposed as the boundary heat flux. In conclusion, the TEG inner heat generation is equal to zero. The TEG unsteady-state heat transfer equation (1) is translated into

$$\rho c_p \frac{\partial T}{\partial \tau} = \lambda \frac{\partial^2 T}{\partial y^2} \tag{2}$$

The corresponding boundary conditions are provided to solve the equation (2). As shown in Fig. 3, the boundary conditions on the cold and hot sides of heat exchanger belong to the third boundary condition. The boundary conditions of other center sides in TEG which are regarded as the interrelated and complementary conditions belong to the second boundary condition. There are the left and right boundary faces on each center side, including $S_{ce,h}$, $S_{cu,h}$, $S_{sl,h}$, $S_{sc,h}$, $S_{sc,c}$, $S_{sl,c}$, $S_{cu,c}$ and $S_{ce,c}$, which are expressed as $S^+_{ce,h}$, $S^-_{ce,h}$, $S^+_{cu,h}$, $S^-_{cu,h}$, $S^+_{sl,h}$, $S^-_{sl,h}$, $S^+_{sc,h}$, $S^-_{sc,h}$, $S^+_{sc,c}$, $S^-_{sc,c}$, $S^+_{sl,c}$, $S^-_{sl,c}$, $S^+_{cu,c}$, $S^-_{cu,c}$, $S^+_{ce,c}$ and $S^-_{ce,c}$ respectively. According to the treatment of Peltier heat and Joule heat, the boundary condition of each part in TEG is listed as following.

(1) On hot side of flow channel ($S_{fc,h}$)

$$-\lambda_{fc} A_{fc} \left.\frac{\partial T}{\partial x}\right|_{x=S_{fc,h}} = h_h A_{ef,fc} \left(T_h - T_{fc,h}\right) \tag{3}$$

(2) On hot side of ceramic substrate ($S_{ce,h}$)

$$-\lambda_{ex} n_{ex} A_{exb} \left.\frac{\partial T}{\partial x}\right|_{x=S^+_{ce,h}} = -\lambda_{ce} n_{ce} A_{ce} \left.\frac{\partial T}{\partial x}\right|_{x=S^-_{ce,h}} \tag{4}$$

(3) On hot side of copper conducting strip ($S_{cu,h}$)

$$-\lambda_{ce} n_{ce} A_{ce} \left.\frac{\partial T}{\partial x}\right|_{x=S^+_{cu,h}} = -\lambda_{cu} n_{cu} A_{cu} \left.\frac{\partial T}{\partial x}\right|_{x=S^-_{cu,h}} - \frac{1}{2} I^2 n_{cu} r_{cu} \tag{5}$$

(4) On hot side of solder layer ($S_{sl,h}$)

$$-\lambda_{cu} n_{cu} A_{cu} \left.\frac{\partial T}{\partial x}\right|_{x=S^+_{sl,h}} + \frac{1}{2} I^2 n_{cu} r_{cu} = -\lambda_{sl} n_{sl} A_{sl} \left.\frac{\partial T}{\partial x}\right|_{x=S^-_{sl,h}} - \frac{1}{2} I^2 n_{sl} r_{sl} \tag{6}$$

(5) On hot side of semiconductor ($S_{sc,h}$)

$$-\lambda_{sl} n_{sl} A_{sl} \left.\frac{\partial T}{\partial x}\right|_{x=S^+_{sc,h}} + \frac{1}{2} I^2 n_{sl} r_{sl} = -\lambda_{sc} n_{sc} A_{sc} \left.\frac{\partial T}{\partial x}\right|_{x=S^-_{sc,h}} - \frac{1}{2} I^2 n_{sc} r_{sc} + n_{sc} \alpha I T_{sc,h} \tag{7}$$

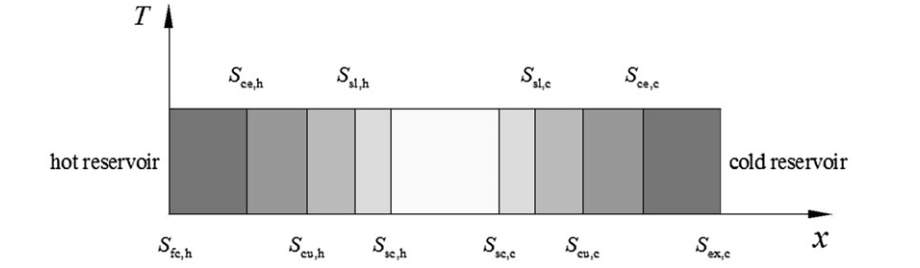


**Fig. 3.** One-dimensional heat transfer model of thermoelectric generator.

(6) On cold side of semiconductor ($S_{sc,c}$)

$$-\lambda_{sc}n_{sc}A_{sc}\left.\frac{\partial T}{\partial x}\right|_{x=S^{+}_{sc,c}}+\frac{1}{2}I^2n_{sc}r_{sc}+n_{sc}\alpha IT_{sc,c}=-\lambda_{sl}n_{sl}A_{sl}\left.\frac{\partial T}{\partial x}\right|_{x=S^{-}_{sc,c}}-\frac{1}{2}I^2n_{sl}r_{sl} \tag{8}$$

(7) On cold side of solder layer ($S_{sl,c}$)

$$-\lambda_{sl}n_{sl}A_{sl}\left.\frac{\partial T}{\partial x}\right|_{x=S^{+}_{sl,c}}+\frac{1}{2}I^2n_{sl}r_{sl}=-\lambda_{cu}n_{cu}A_{cu}\left.\frac{\partial T}{\partial x}\right|_{x=S^{-}_{sl,c}}-\frac{1}{2}I^2n_{cu}r_{cu} \tag{9}$$

(8) On cold side of copper conducting strip ($S_{cu,c}$)

$$-\lambda_{cu}n_{cu}A_{cu}\left.\frac{\partial T}{\partial x}\right|_{x=S^{+}_{cu,c}}+\frac{1}{2}I^2n_{cu}r_{cu}=-\lambda_{ce}n_{ce}A_{ce}\left.\frac{\partial T}{\partial x}\right|_{x=S^{-}_{cu,c}} \tag{10}$$

(9) On cold side of ceramic substrate ($S_{ce,c}$)

$$-\lambda_{ce}n_{ce}A_{ce}\left.\frac{\partial T}{\partial x}\right|_{x=S^{+}_{ce,c}}=-\lambda_{ex}n_{ex}A_{ex}\left.\frac{\partial T}{\partial x}\right|_{x=S^{-}_{ce,c}} \tag{11}$$

(10)On cold side of flow channel ($S_{fc,c}$)

$$-\lambda_{ex}A_{ef,ex}\left.\frac{\partial T}{\partial x}\right|_{x=S_{ex,c}}=h_cA_{ef,ex}(T_{ex,c}-T_c) \tag{12}$$

where $\lambda_{fc}$, $\lambda_{ce}$, $\lambda_{cu}$, $\lambda_{sl}$, $\lambda_{sc}$ and $\lambda_{ex}$ are thermal conductivities of flow channel, ceramic substrate, copper conducting strip, solder layer, semiconductor and heat exchanger, respectively. $A_{ce}$, $A_{cu}$, $A_{sl}$, $A_{sc}$ and $A_{ex}$ are cross sectional areas of ceramic substrate, copper conducting strip, solder layer, semiconductor and heat exchanger, respectively; $n_{ce}$, $n_{cu}$, $n_{sl}$, $n_{sc}$ and $n_{ex}$ are numbers of ceramic substrate, copper conducting strip, solder layer, semiconductor and heat exchanger, respectively; $r_{cu}$, $r_{sl}$ and $r_{sc}$ are electric resistances of copper conducting strip, solder layer and semiconductor, respectively; $T_h$ and $T_c$ are temperatures of hot reservoir and cold reservoir, respectively. $T_{fc,h}$ is hot side temperature of flow channel, $T_{ex,c}$ is cold side temperature of heat exchanger, and $A_{ef,fc}$ and $A_{ef,ex}$ are the effective areas of flow channel and heat exchanger which are expressed as respectively

$$A_{ef,fc}=n_{ce}A_{ce} \tag{13}$$

$$A_{ef,ex}=A_{ex,b}+\eta_fA_{ex,f} \tag{14}$$

where $A_{ex,b}$ and $A_{ex,f}$ are surface areas of heat exchanger base and fin respectively, and $\eta_f$ is fin efficiency of heat exchanger. And the fin efficiency is given as

$$\eta_f=\frac{\mathrm{th}(mH_f)}{mH_f} \tag{15}$$

where th is hyperbolic tangent function, $H_f$ is the height of fin, and $m$ is a constant which is calculated by

$$m=\sqrt{\frac{h_cP_f}{\lambda_{ex}A_f}} \tag{16}$$

where $P_f$ and $A_f$ are perimeter and area of cross section of fin respectively, and $h_c$ is coefficient of convective heat transfer on cold side of heat exchanger. While $h_h$ in equation (3) is coefficient of convective heat transfer on hot side of flow channel. The two coefficients are solved by

$$h=\frac{Nu\lambda}{l_{ch}} \tag{17}$$

where $l_{ch}$ is characteristic length, and $Nu$ is Nusselt number. Because the structures of the convective heat transfer are different, the equation of Nusselt number of hot side of flow channel is different from that of cold side of heat exchanger.

For internal pipe flow of hot fluid, the Nusselt number is expressed best by Gnielinski correlation [20]

$$Nu_h=\frac{(f/8)(Re_h-1000)Pr_h}{1+12.7\sqrt{f/8}\left(Pr_h^{2/3}-1\right)}\left[1+\left(\frac{l_{ch,fc}}{l_{fc}}\right)^{2/3}\right],\quad Re_h=2300\sim10^6 \tag{18}$$

where $Re_h$ and $Pr_h$ are Reynolds number and Prandtl number of hot reservoir respectively, $l_{fc}$ and $l_{ch,\ fc}$ are length and characteristic length of flow channel respectively, and $f$ is Darcy resistance coefficient of turbulent tube flow. $l_{ch,\ fc}$, $Re_h$ and $f$ are given respectively by

$$l_{ch,fc}=\frac{4A_{fc}}{P_{fc}} \tag{19}$$

$$Re_h=\frac{u_hl_{ch,fc}}{\nu_h} \tag{20}$$

$$f=(1.82\lg Re_h-1.64)^{-2} \tag{21}$$

where $P_{fc}$ and $A_{fc}$ are perimeter and area of cross section of flow channel respectively, $\nu_h$ is kinematic viscosity coefficient of hot reservoir, and $u_h$ is velocity of hot reservoir which is expressed as

$$u_h=\frac{W_h}{A_{fc}} \tag{22}$$

where $W_h$ is the flow rate of hot reservoir.

For the external cooling air flow, a fined heat exchanger is showed in Fig. 4. The expression of the Nusselt number can be calculated by Ref. [21]

$$\begin{aligned}Nu_c&=0.664Re_c^{1/2}Pr_c^{1/3},\ Re_c<5\times10^5(\text{Laminar flow})\\ Nu_c&=0.037Re_c^{4/5}Pr_c^{1/3},\ Re_c\geq5\times10^5(\text{Turbulent flow})\end{aligned} \tag{23}$$

where $Re_c$ and $Pr_c$ are Reynolds number and Prandtl number of cold reservoir, respectively. $Re_c$ is given by

$$Re_c=\frac{u_cl_{ch,ex}}{\nu_c} \tag{24}$$

where $l_{ch,\ fc}$ is the characteristic length of heat exchanger which can be taken as the height of fins [17], $\nu_c$ is kinematic viscosity coefficient of cold reservoir, and $u_c$ is velocity of cold reservoir, which is expressed as

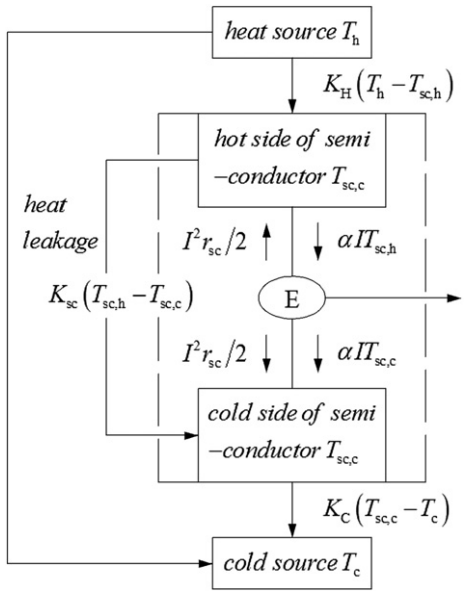


**Fig. 4.** Structure diagram of heat transfer system of thermoelectric generator.

$$u_c = \frac{W_c}{A_f} \tag{25}$$

where $W_c$ is flow rate of cold reservoir, and $A_f$ is the passageway area between fins.

### 2.2. Performance calculation model

The TEG output performance is evaluated by calculating output power and the system efficiency [2]. According to Seebeck effect, the electromotive force of thermoelectric circuit is expressed by

$$E(\tau) = n\alpha[T_{sc,h}(\tau) - T_{sc,c}(\tau)] \tag{26}$$

where $T_{sc,h}$ and $T_{sc,c}$ are the hot and cold side temperatures of semiconductor respectively, $n$ is the number of thermoelectric couple, and $\alpha$ is Seebeck coefficient. The current of thermoelectric circuit is

$$I(\tau) = \frac{E(\tau)}{r_i + r_{con} + r_L} \tag{27}$$

where $r_i$, $r_{con}$, and $r_L$ are inner electric resistance, contact electric resistance and load electric resistance, respectively. So the output power is given by

$$P_L(\tau) = I^2 r_L = \frac{n^2\alpha^2[T_{sc,h}(\tau) - T_{sc,c}(\tau)]^2}{(r_i + r_{con} + r_L)^2} r_L \tag{28}$$

When load electric resistance is equal to the matched electric resistance, the output power reaches maximum. So the matched electric resistance is solved to obtain the maximal output power. The expression of the matched electric resistance is deduced in the steady condition as follows.

Fig. 4 presents semiconductor absorbing heat from hot reservoir and releasing heat to cold reservoir. According to thermodynamic theory, semiconductor can regarded as heat engine working between hot reservoir and cold reservoir, which is the dotted part in Fig. 4. Based on Fourier Law, the heat which semiconductor absorbs from hot reservoir and releases to cold reservoir is expressed as

$$Q_{sc,h} = nK_H(T_h - T_{sc,h}) \tag{29}$$

$$Q_{sc,c} = nK_C(T_{sc,c} - T_c) \tag{30}$$

where $K_H$ is the thermal conductance from hot reservoir to hot side of semiconductor, and $K_C$ is the thermal conductance from cold reservoir to cold side of semiconductor. $K_H$ and $K_C$ are given by

$$K_H = \frac{1}{1/K_h + 1/K_{fc} + 1/K_{ce} + 1/K_{cu} + 1/K_{sl} + R_{con}} \tag{31}$$

$$K_C = \frac{1}{1/K_c + 1/K_{ex} + 1/K_{ce} + 1/K_{cu} + 1/K_{sl} + R_{con}} \tag{32}$$

where $K_h$ is thermal conductance from hot reservoir to hot side of flow channel, $K_c$ is thermal conductance from cold reservoir to cold side of heat exchanger, $K_{fc}$, $K_{ce}$, $K_{cu}$, $K_{sl}$ and $K_{ex}$ are thermal conductance of flow channel, ceramic substrate, copper conducting strip, solder layer and heat exchanger respectively, and $R_{con}$ is the TEM contact thermal resistance.

In addition, Peltier effect shows up as heat absorption on hot side and heat release on cold side of semiconductor, and Joule effect shows up as heat release on hot and cold sides of semiconductor. As showed in Fig. 4, $Q_{sc,h}$ and $Q_{sc,c}$ are also given by

$$Q_{sc,h} = n\left[\alpha I T_{sc,h} - \frac{1}{2}I^2(r_{sc} + r_{sl,sc}) + K_{sc}(T_{sc,h} - T_{sc,c})\right] \tag{33}$$

$$Q_{sc,c} = n\left[\alpha I T_{sc,c} + \frac{1}{2}I^2(r_{sc} + r_{sc,sl}) + K_{sc}(T_{sc,h} - T_{sc,c})\right] \tag{34}$$

where $r_{sc}$ and $K_{sc}$ are electric resistance and thermal conductance of a couple of semiconductors respectively, $r_{sl,sc}$ is contact electric resistance between solder layer and semiconductor on the hot side, and $r_{sc,sl}$ is contact electric resistance between semiconductor and solder layer on the cold side.

The heat loss is neglected when the TEG heat transfer model is taken as one-dimensional model. Based on energy conversation law, the heat semiconductor releases to cold reservoir and the output power add up to the heat semiconductor absorbs from hot reservoir:

$$Q_{sc,h} = Q_{sc,c} + P_L \tag{35}$$

Combine (25) to (35),

$$\Delta T_{sc} = T_{sc,h} - T_{sc,c} = \frac{(T_h - T_c)(r_i + r_{con} + r_L)}{Bn^2\alpha^2 + A(r_i + r_{con} + r_L)} \tag{36}$$

where

$$A = 1 + \left(\frac{1}{K_H} + \frac{1}{K_C}\right)K_{sc} \tag{37}$$

$$B = \frac{T_h}{K_C} + \frac{T_c}{K_H} \tag{38}$$

Substitute (36) to (28)

$$P_L = \frac{n^2\alpha^2 r_L(T_h - T_c)^2}{\left[Bn^2\alpha^2 + (r_i + r_{con} + r_L)A\right]^2} \tag{39}$$

The equation (39) is taken the derivative with respect to load resistance. Then let the derivative equation be equal to zero,

$$\frac{\partial P_L}{\partial r_L} = 0 \tag{40}$$

Therefore, the matched load resistance can be obtained

$$r_m = r_i + r_{con} + \frac{Bn^2\alpha^2}{A} \tag{41}$$

Substitute (41) to (28), the maximal output power is

$$P_{max}(\tau) = \frac{n^2\alpha^2\left(A^2 r_i + ABn^2\alpha^2\right)\left[T_{sc,h}(\tau) - T_{sc,c}(\tau)\right]^2}{\left(2Ar_i + Bn^2\alpha^2\right)^2} \tag{42}$$

According to Newton's law of cooling, the TEG heat absorption capacity is

$$Q_h(\tau) = h_h A_{fc}\left[T_h(\tau) - T_{ex,h}(\tau)\right] \tag{43}$$

Finally, the TEG system efficiency is calculated by

$$\eta(\tau) = \frac{P_{max}(\tau)}{Q_h(\tau)} = \frac{n^2\alpha^2\left(A^2 r_i + ABn^2\alpha^2\right)\left[T_{sc,h}(\tau) - T_{sc,c}(\tau)\right]^2}{h_h A_{ef}\left(2Ar_i + Bn^2\alpha^2\right)^2\left[T_h(\tau) - T_{ex,h}(\tau)\right]} \tag{44}$$

The performance calculation model is built by deducing the expressions (42) and (44). So the TEG dynamic model has been setup with the addition of the unsteady-state heat transfer model.

## 3. Experimental validation

### 3.1. Experimental setup

An experimental setup which is designed to validate the TEG dynamic model has been established. The physical and schematic diagrams of the setup are shown in Figs. 5 and 6, respectively. The system consists of a thermoelectric converter, a hot fluid loop, a cooling device and a data acquisition system.

In the hot fluid loop, a single stainless steel channel (600 mm × 100 mm × 18 mm, and 2 mm wall thickness), which hot water flows through, is lined on each side with eighteen thermoelectric modules (TEC1-12708-NET1, a kind of thermoelectric cooling module with 127 thermoelectric couples, and 40 mm length, 40 mm width and 3.5 mm height). All the modules are connected electrically in series. Hot water that is used to simulate waste heat is supplied by the circulating constant temperature bath (temperature range: room temperature − 100 °C). A water circulating pump is located to monitor the flow rate of hot water. And the air cooling is used on the cold side. To enhance the heat dissipation, six heat exchangers are fixed on the cold side of the modules. At the same time, two fans are installed on the heat exchanger for the forced-convection heat transfer.

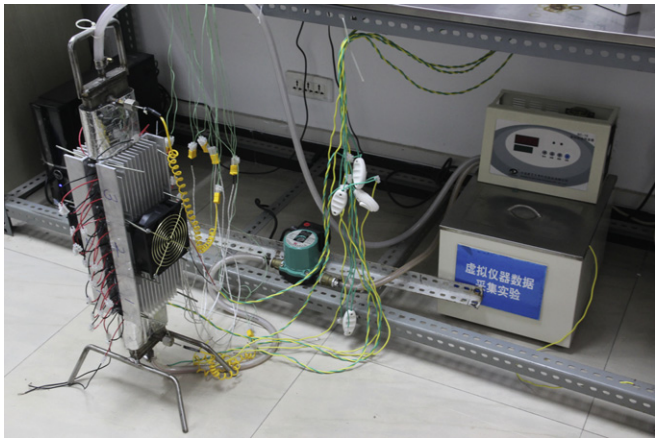


**Fig. 5.** Physical diagram of the experimental setup of TEG applied in waste heat recovery.

In addition, there are eight thermocouples used in data acquisition system. As shown in Fig. 5, two thermocouples are located at the inlet and outlet of flow channel, and other thermocouples are located averagely on both surfaces of thermoelectric module in one side of flow channel. In order to measure the temperature in real time, a series of virtual instruments from National Instruments Corporation (NI) are employed here.

### 3.2. Comparison of simulation and experimental results

Experiments are conducted under the specific operating conditions as follows: the temperature of hot water is between 50 °C and 90 °C, the air temperature is constant 28.5 °C, and the flow rates of hot and cold fluid are 2.76 $m^3$/h and 43.2 $m^3$/h, respectively. Besides, the physical parameters and dimension parameters of each part in TEG are listed in Tables 1 and 2.

Out of flatness of the contact surface between TEM and the convective heat transfer system that is caused by the installment of thermocouples, the contact thermal resistance is so large that it has to be considered into the model. The contact thermal resistance can be gained by experiment, and be replaced by the corresponding thermal resistance of grease with approximately $8.6 \times 10^{-4}$ m of thickness and 1.5 W $m^{-2}$ $K^{-1}$ of thermal conductivity in the simulating process. Meanwhile, the contact electric resistance needs to be calculated for the reason that the number of thermoelectric modules is large enough, even if a single module has a small contact electric resistance. The matched load resistance can be gained by experiment. So the whole TEG contact electric resistance can be calculated by the expression (41). Finally, the calculated value of the contact electric resistance is approximately 6 Ω.

To compare simulated results with experimental data, the simulation must have the same operating conditions as the experiment besides based on an accuracy system model. Each experiment is repeated at least three times to obtain reproducible results. And the mean vale of the three effective experimental results acts as the final experimental data. Here, the TEM ceramic surface temperatures and output power are regarded as the study objects. These comparisons are shown in Figs. 7 and 8.

Fig. 7 shows the temperature variations on the hot and cold ceramic surfaces with different hot fluid temperatures in steady states. The steady states mean the TEG temperature distribution remains constant with time. Furthermore, because Peltier effect and Joule effect reach the maximum in a short circuit, they have the maximum impact on TEG temperature distribution right now. So Fig. 7 is gained in a short circuit. As it can be seen in Fig. 7, the experimental results nearly coincide with the simulation results. The experimental temperatures on the hot side are a little lower than the simulated temperatures. And the maximum value of variation is within 2 °C.

Output power versus load resistance at three different hot fluid temperatures is plotted in Fig. 8. All the simulated results are a little higher than the experimental data. However, the relative error between experimental and simulated results is within 20%. At hot fluid temperature of 90 °C, the error is only 1.9%.

Therefore, the steady-state simulated results and experimental data shown in Figs. 7 and 8 indicate not only a very similar trend, but also acceptable relative errors. It is demonstrated that the simulated results are in good agreement with the experimental data in the steady-state operation, so the reasonability of TEG dynamic model is partially verified.

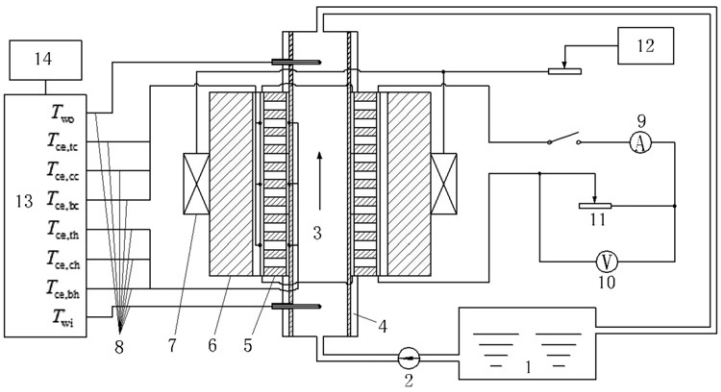


**Fig. 6.** Schematic diagram of the experimental setup of TEG applied in waste heat recovery.

## 4. Dynamic simulation

Based on the established dynamic model, the dynamic response characteristics of surface temperatures of semiconductor, maximum output power and system efficiency are studied when temperatures or flow rates of heat reservoir generate step changes. The initial condition in which TEG operates can be proposed as follows: hot water temperature is 60 °C, air temperature is 30 °C, and flow rates of water and air are 1.38 $m^3\ h^{-1}$ and 21.6 $m^3\ h^{-1}$, respectively.

### *4.1. Dynamic characteristic with step change of heat reservoir temperature*

Fig. 9 presents the dynamic response characteristics of hot and cold semiconductor surface temperatures with step changes of heat reservoir temperatures. There are four step changes in total as shown in Fig. 9. To analyze the influence of each step change on TEG clearly, the set value of the time interval between two adjacent step changes must assure each temperature in TEG reaches at least 99% of the steady-state value. And the TEG state is called as the quasi-equilibrium state right now. Here, it is found that the time interval can be set as 400 s to reach this state by simulating. The first step change is hot water temperature jumping from 60 °C to 70 °C at the time of zero. Secondly, hot water temperature follows a step change from 70 °C to 60 °C. Thirdly, air temperature follows a step change from 30 °C to 20 °C. Lastly, air temperature returns to 30 °C in the way of step change.

As shown in Fig. 9, the hot semiconductor surface temperature increases nearly to the steady-state value in a surprisingly short time, and the cold semiconductor surface temperature increases slowly compared with the hot semiconductor surface temperature at the first stage. At the second stage, the variations are identical but the change directions are opposite to those at the first stage for the hot and cold semiconductor surface temperatures. Both the hot and cold semiconductor side temperatures display an exponential decay, but the decrease of the cold side temperature is bigger than that of the hot side temperature at the third stage. The relationship of the response characteristics between the fourth and the third stage is just like that between the second and the first stage.

Since the thermal resistance from hot reservoir to hot side of semiconductor is very small, hot side temperature of semiconductor possesses the characteristic of increasing rapidly at the first stage. The main reason may be due to that the thermal resistance of semiconductor occupies a considerable proportion in the whole thermal resistance. Based on the trends of the hot and cold semiconductor surface temperatures, the trend of the temperature difference between the two surfaces shown in Fig. 9 is then easy to understand. In addition, the response time of the hot semiconductor surface temperature at the first stage is much shorter than that of the cold semiconductor surface temperature at the third stage. According to heat transfer theory, this phenomenon can be explained by the much larger the convective heat transfer coefficient in hot reservoir than that in cold reservoir.

Fig. 10 shows the response characteristics of maximum output power and system efficiency at the same operating conditions with Fig. 9. It can be seen that maximum output power reaches a peak in a short time, then decreases slowly to a stable value at the first stage. It is clearly shown in Figs. 9 and 10 the whole tendency of

**Table 1**
Basic physical parameters of each component in thermoelectric generator.

| Parts | Specific heat capacity J/(kg·K) | Thermal conductivity W/(m·K) | Density kg/m3 | Electrical resistivity Ω m |
|---|---|---|---|---|
| Semiconductor | 158 | 1.5 | 7300 | $1 \times 10^{-5}$ |
| Solder layer | 167 | 33 | 8560 | $5 \times 10^{-7}$ |
| Copper conducting strip | 386 | 398 | 8930 | $2 \times 10^{-8}$ |
| Ceramic substrate | 765 | 36 | 3975 | – |
| Flow channel | 644 | 12 | 7600 | – |
| Heat exchanger | 871 | 162 | 2660 | – |

'–' In table means the parameter needn't to be used in calculation.

**Table 2**
Dimensions of each component in thermoelectric generator.

| Parts | Cross section length mm | Cross section width mm | Height mm | Number |
|---|---|---|---|---|
| Semiconductor | 1.47 | 1.47 | 1.3 | $4 \times 2 \times 127$ |
| Solder layer | 1.47 | 1.47 | .05 | $4 \times 2 \times 127$ |
| Copper conducting strip | 4 | 1.6 | .4 | $4 \times 127$ |
| Ceramic substrate | 40 | 40 | .65 | 4 |
| Flow channel | 100 | 18 | 600 | 1 |
| Heat exchanger base | 80 | 80 | 6 | 1 |
| Heat exchanger fin | 80 | 4 | 38 | 8 |

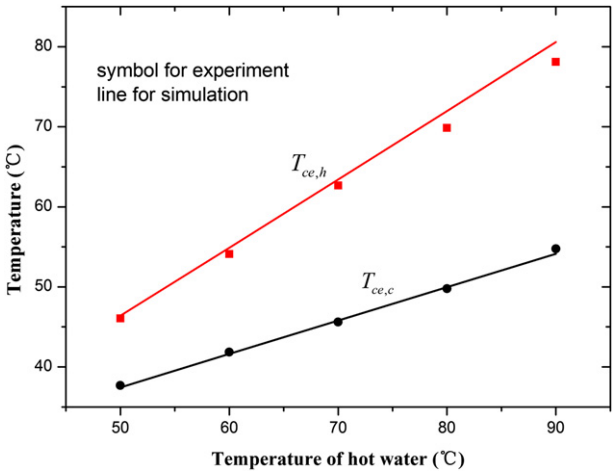


**Fig. 7.** Experimental data and simulating results for the hot and cold ceramic surface temperatures versus hot water temperature in the steady-state operation.

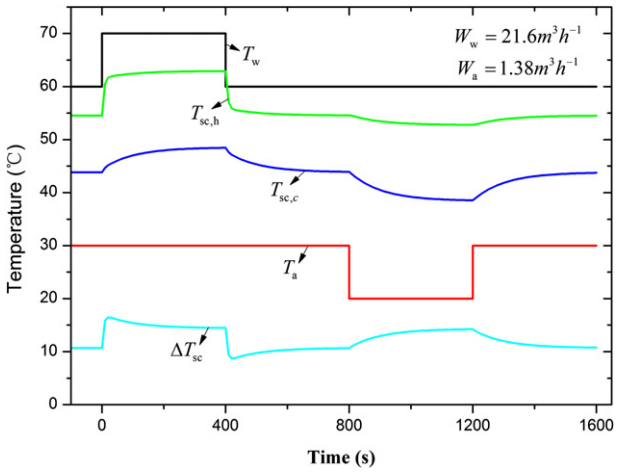


**Fig. 9.** Hot and cold semiconductor surface temperatures versus time with step changes of heat reservoir temperatures.

maximum output power are consistent with that of the temperature difference in hot side and cold side of semiconductor. This result can be explained by the expression (42).

Though the heat input of the thermoelectric converter will change when the heat reservoir temperatures make step changes, its relative variation is much lower than that of output power. Hence, system efficiency variation depends mainly on the variation of output power. The reason causing the oscillations is that the heat transfer rate is finite so that hot side temperature of flow channel cannot respond as quickly as hot water temperature.

### 4.2. *Dynamic characteristic with step change of heat reservoir flow rate*

The dynamic response characteristics of semiconductor surface temperatures, maximum output power and system efficiency with step changes of heat reservoir flow rates are described in Figs. 11 and 12. Each step change of heat reservoir flow rates takes place at the same moment as the corresponding step change of heat reservoir temperatures. The first two change steps are that flow rate of hot water makes a round trip between 1.38 $m^3$ $h^{-1}$ and 2.76 $m^3$ $h^{-1}$. In this process, flow rate of air follows the third step change from 21.6 $m^3$ $h^{-1}$ to 43.2 $m^3$ $h^{-1}$, which returns to 21.6 $m^3$ $h^{-1}$ at the fourth step change. It is found that the curves in Figs. 11 and 12 have the same trend as those in Figs. 9 and 10, respectively. Accordingly, adding flow rate of hot water could generate a similar impact with increasing its temperature on TEG; while for cooling air, adding flow rate has a similar impact on decreasing its temperature.

It can be seen in Fig. 12, though both flow rates of water and air have changed, the variation of maximum output power and system efficiency at the last two stages are larger than those at the first two stages. This result shows enhancing heat dissipation on cold side generates a greater improvement on TEG output performance.

Finally, combining the above figures, it can be seen that the whole tendencies of maximum output power and system efficiency are mostly consistent with that of the corresponding temperature difference between hot side and cold side of the semiconductor. On this view, TEG output performance is mainly depended on the temperature difference between hot side and cold side of the semiconductor. When the temperature difference increases, TEG output performance can be improved. In addition, when hot water temperature or flow rate change rapidly, output power generates a sharp change remarkably. Therefore, in order to protect electric equipment, it needs to avoid or reduce the variation of output power generated by fluctuation of hot reservoir in system design and operation.

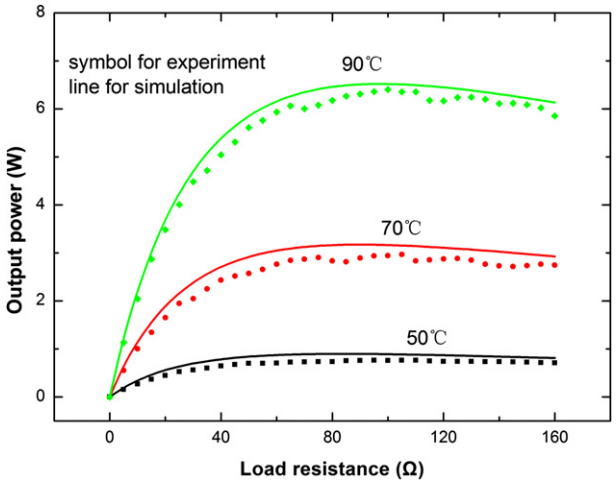


**Fig. 8.** Experimental data and simulating results for output power versus load resistance for three different hot water temperatures in the steady-state operation.

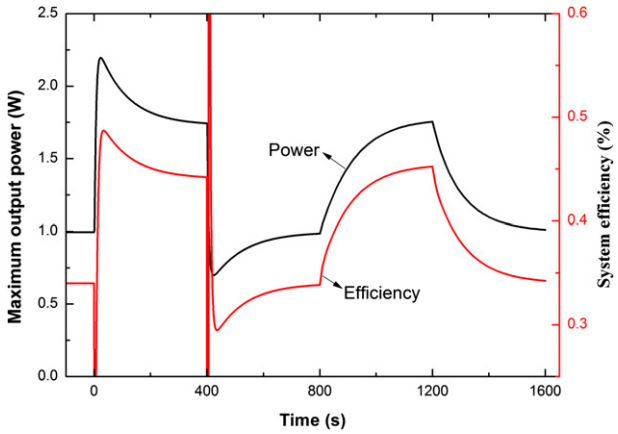


**Fig. 10.** Maximum output power and system efficiency versus time with step changes of heat reservoir temperatures.

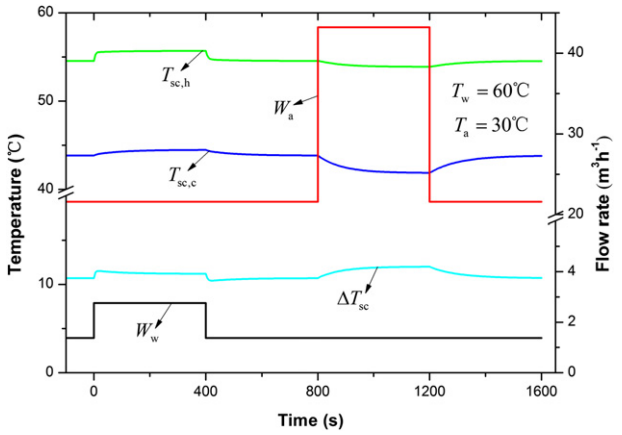


**Fig. 11.** Hot and cold semiconductor surface temperatures versus time with step changes of flow rates.

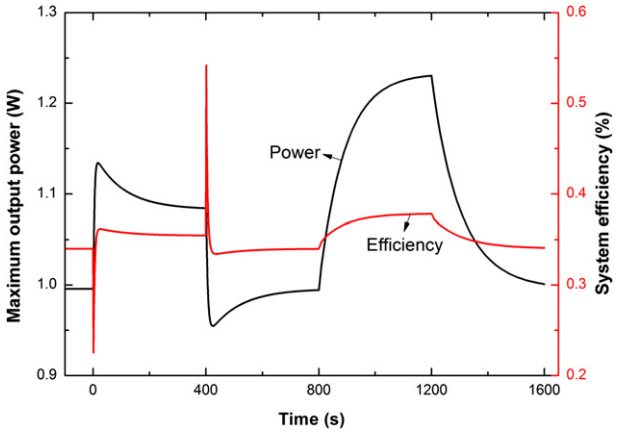


**Fig. 12.** Maximum output power and system efficiency versus time with step changes of flow rates.

## 5. Conclusion

In this study, a theoretic dynamic model of a general thermoelectric generator with finned heat exchangers is presented, and a waste heat recovery thermoelectric generator experimental setup has been constructed to validate this model. The good agreement between the steady-state simulated results and experimental data has approved the reasonability of the system dynamic model. Therefore, this system model can be used in dynamic simulation.

By means of step changes of heat reservoir temperatures and flow rates, the dynamic response characteristics of temperatures on the hot and cold semiconductor surfaces, maximum output power and system efficiency are studied. The TEG output performance has different dynamic characteristics at different operating conditions. There are two conclusions obtained as follows:

a. Compared with enhancing heat transfer on hot side, enhancing heat dissipation on cold side generates a greater improvement on TEG output performance.

b. In order to protect electric equipment, it is necessary to avoid or reduce the variation of output power generated by fluctuation of hot reservoir in system design and operation.

Therefore, these dynamic simulation results, gained by employing the dynamic model to analyze different operating conditions, could provide guidelines for performance optimization and safe operation of thermoelectric generator. The results have provided a useful guideline for designing TEGs.

## Acknowledgment

This research was supported by National Natural Science Foundation of China (Grant No. 51276206) and the Fundamental Research Funds for the Central Universities (No. CDJZR10140005).

## References

[1] Riffat SB, Ma X. Thermoelectrics: a review of present and potential applications. Appl Therm Eng 2003;23(8):913–35.
[2] Niu X, Yu J, Wang S. Experimental study on low-temperature waste heat thermoelectric generator. J Power Sources 2009;188(2):621–6.
[3] Casano G, Piva S. Experimental investigation of the performance of a thermoelectric generator based on Peltier cells. Exp Therm Fluid Sci 2011;35(4):660–9.
[4] Liang G, Zhou J, Huang X. Output characteristics analysis of thermoelectric generator based on accurate numerical model. In: Proceeding of the second International Conference on Asia-Pacific Power and Energy Engineering Chengdu; 2010.
[5] Hsiao YY, Chang WC, Chen SL. A mathematic model of thermoelectric module with applications on waste heat recovery from automobile engine. Energy 2010;35(3):1447–54.
[6] Zhou Y. Optimal design of a new type of semiconductor thermoelectric generator. J Xiamen Univ 2001;40(2):882–7 [in Chinese].
[7] Chen LG, Li J, Sun FR, Wu C. Performance optimization of two-stage semiconductor thermoelectric-generators. Appl Energ 2005;82(4):300–12.
[8] Chen LG, Meng FK, Sun FR. A novel configuration and performance for two-stage thermoelectric heat pump system driven by two-stage thermoelectric generator. Proc IMechE, Part A: J Power Energ 2009;223(A4):329–39.
[9] Chen LG, Gong JZ, Wu C, Sun FR. Effect of heat transfer on the performance of thermoelectric generator. Int J Therm Sci 2002;41(1):95–9.
[10] Chen LG, Sun FR, Wu C. Heat transfer surface area optimization for a thermoelectric generator. Int J Ambient Energ 2007;28(3):135–42.
[11] Meng FK, Chen LG, Sun FR. Effect of temperature dependences of thermoelectric properties on the power and efficiency of a multielement thermoelectric generator. Int J Energ Environ 2012;3(1):137–50.
[12] Chen LG, Sun FR, Wu C. Thermoelectric generator with linear phenomenological heat transfer law. Appl Energ 2005;81(4):358–64.
[13] Meng FK, Chen LG, Sun FR. Performance characteristics of the multielement thermoelectric generator with radiative heat transfer law. Int J Sustain Energ 2012;31(2):119–31.
[14] Hsu CT, Huang GY, Chu HS, Yu B, Yao DJ. Experiments and simulations on low-temperature waste heat harvesting system by thermoelectric power generators. Appl Energ 2011;88(4):1291–7.
[15] Crane DT, Jackson GS. Optimization of cross flow heat exchangers for thermoelectric waste heat recovery. Energ Convers Manag 2004;45(9):1565–82.
[16] Gou XL, Xiao H, Yang SW. Modeling, experimental study and optimization on low-temperature waste heat thermoelectric generator system. Appl Energ 2010;10(87):3131–6.
[17] Meng FK, Chen LG, Sun FR. A numerical model and comparative investigation of a thermoelectric generator with multi-irreversibilities. Energy 2011;36(5):3513–22.
[18] Yang QS. Advanced heat transfer. 2nd ed. Shanghai: Shanghai Jiaotong University; 2001 [in Chinese].
[19] Cvahte M, Srtnad J. A thermoelectric experiment in support of the second law. Eur J Phys 1988;9(1):11–7.
[20] Yang SM, Tao WQ. Heat transfer. 4th ed. Beijing: Higher Education; 2006 [in Chinese].
[21] Cengel Y. Heat transfer: a practical approach. 2nd ed. New York: McGraw-Hill; 2002.